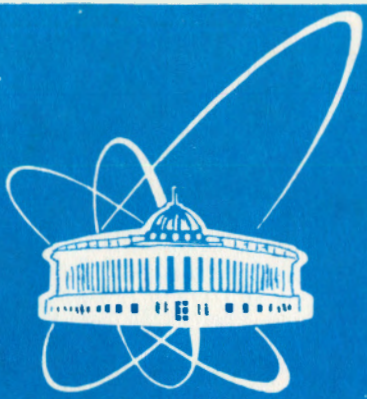

ОБЪЕДИНЕННЫЙ
ИНСТИТУТ
ЯДЕРНЫХ
ИССЛЕДОВАНИЙ

Дубна

98-98

E2-98-98

G.N.Afanasiev*, V.G.Kartavenko, E.N.Magar

VAVILOV–CHERENKOV RADIATION IN DISPERSIVE MEDIUM

Submitted to «Physica B»

*E-mail: afanasev@thsun1.jinr.dubna.su

1998

1 Introduction

The specific electromagnetic radiation produced by fast electrons moving in medium was observed by P.A. Cherenkov in 1934 [1]. Tamm and Frank [2] considered the motion of a point charge in medium with a constant electric permittivity. They showed that the charge should radiate when its velocity exceeds the light velocity in medium. For the frequency independent electric permittivity the electromagnetic strengths have δ-type singularities on the surface of the so-called Cherenkov (or Mach) cone [3-6]. This leads to the divergence of the integrals involving the product of electromagnetic strengths. In particular, this is true for the total flux of electromagnetic field (EMF). To avoid this difficulty Tamm and Frank (see, e.g., Frank's book [7]) made the Fourier transformation of EMF and integrated the energy flux up to some maximal frequency ω_0.

The goal of this treatment is to consider consequences arising from the uniform motion of a charge in the nonmagnetic medium described by the frequency-dependent one-pole electric permittivity

$$\epsilon(\omega) = 1 + \frac{\omega_L^2}{\omega_0^2 - \omega^2} \tag{1.1}$$

and its complex counterpart

$$\epsilon(\omega) = 1 + \frac{\omega_L^2}{\omega_0^2 - \omega^2 + ip\omega}. \tag{1.2}$$

These expressions are suitable extrapolations between the static case $\omega = 0$, $\epsilon(\omega) = \epsilon_0 = 1 + \omega_L^2/\omega_0^2$ and the high-frequency limit $\omega = \infty$, $\epsilon(\omega) = 1$. In the usual interpretation ω_L and ω_0 are the plasma frequency $\omega_L^2 = 4\pi N_e e^2/m$ (N_e is the number of electrons per unit of volume, m is the electron mass) and some resonance frequency. Quantum-mechanically, it can be associated with the energy excitation of the lowest atomic level. Our subsequent exposition does not depend on this particular interpretation of ω_L and ω_0.

In what follows we shall use the quantity $\beta_c = 1/\sqrt{1 + \omega_L^2/\omega_0^2}$. It plays a major role even if the frequency dependence of ϵ is taken into account. In the absence of dispersion it coincides with the light velocity in medium. It is seen that β_c changes from $\beta_c = 0$ for $N >> 1$ up to $\beta_c = 1$ for $N = 0$. We refer to these limit cases as to optically dense and rarefied media, resp.

Equations (1.1) and (1.2) are standard parametrizations describing a lot of optical phenomena [8]. They are valid when the wavelength of the EMF is much larger than the distance between the particles of medium on which the light scatters. The typical atomic dimensions are of an order of $a \approx \hbar/mc\alpha$; $\alpha = e^2/\hbar c$, m is the electron mass. This gives $\lambda = c/\omega >> a$ or $\omega << mc^2\alpha/\hbar \approx 5 \cdot 10^{18} sec^{-1}$. The typical atomic frequencies are of the order $\omega_0 \approx mc^2/\hbar\alpha^2 \approx 10^{16} sec^{-1}$. As $\omega << \omega_0$, the physical region extends well beyond ω_0. For $\omega >> \omega_0$, $\epsilon(\omega) \approx 1$, that is, medium oscillators have no enough time to

be excited. Following the book [9] and review [10] we extrapolate parametrizations (1.1) and (1.2) to all ω. This means that we disregard excitation of nuclear levels and discrete structure of scatterers.

In Eq. (1.1), $\epsilon(\omega)$ is negative for $\omega_0^2 < \omega^2 < \omega_0^2 + \omega_L^2$. For the free electromagnetic wave this leads to its space damping in this ω region even for real $\epsilon(\omega)$ (see, e.g., [9]). For the EMF radiated by a moving charge the conditions for EMF damping are modified (see sections 3 and 4).

Strictly speaking, Eqs. (1.1) and (1.2) are valid for media with $\epsilon_0 \approx 1$ (e.g., for gases). In what follows we apply Eqs. (1.1) and (1.2) to fictitious medium with $\beta_c = 0.8$, $n = \sqrt{\epsilon_0} = 1/\beta_c = 1.25$. For such a value of the refractive index n one should use Clausius-Mossotti (or Lorentz-Lorenz) formula [13]. However, as it was admitted in [14], the qualitative predictions are the same for both these representations of ϵ. As our consideration is pure qualitative at this stage, we restrict ourselves to the ϵ representations (1.1) and (1.2).

We intend to consider the effects arising from the uniform charge motion in medium with $\epsilon(\omega)$ given by (1.1) and (1.2). Partly this was done by E. Fermi in 1940 [11]. He showed that a charged particle moving uniformly in medium with permittivity (1.1) should radiate at every velocity. He also showed that energy losses as a function of the charge velocity are less than those predicted by the Bohr theory [12].

However, the following questions remained unanswered:

1. How the EMF strengths and energy flux are distributed in space? In particular, what is their angular distribution?
2. How these distributions depend on the charge velocity? In particular, how the transition takes place from the subluminal regime to the superluminal one?
3. How the value of parameter the p defining the imaginary part of ϵ affects the energy losses, electromagnetic strengths, etc.?

In this consideration we restrict ourselves to the classical theory of the Vavilov-Cherenkov radiation with electric permittivity given by (1.1) and (1.2). It is suggested that uniform motion of a particle is maintained by some external force the origin of which is not of interest for us.

The plan of our exposition is as follows.

In section 2, necessary mathematical formulae are presented.

In section 3, we present in a manifestly real form the electromagnetic potentials and field strengths for a charge moving uniformly in a dielectric with $\epsilon(\omega)$ given by (1.1).

In section 4, we evaluate the energy losses as a function of the charge velocity for ϵ given by (1.1). This dependence shows that the moving charge radiates at each velocity. In the same section, we demonstrate how the energy flux is distributed over the surface of a cylinder coaxial with the charge trajectory. It is shown that for the charge velocity greater than some critical one (we designate it as v_c) the main contribution to the energy flux comes from the space region where in the absence of ω dispersion the Cherenkov cone

intersects the cylinder surface. The rapid oscillations of the energy flux are observed in this region. For $v < v_c$ this space region contributes practically nothing to the energy flux. This seems to be in conflict with the energy losses obtained earlier [14].

This inconsistency is discussed in section 5. Using the WKB approach as a rough estimate we show that for $v < v_c$ main contribution to the energy losses comes from the space region sufficiently remote from the one mentioned above and lying behind a moving charge. A posteriori we confirm this by direct calculations presented in sect. 6. In the same section, we use these results as a hint for the explanation of experiments discussed recently in [15-17].

In section 7, we analyze how the radiated energy flux and its space distribution depend on the value of the parameter p defining the imaginary part of ϵ. It turns out that for $v < v_c$ the radiated energy flux is damped much stronger than for $v > v_c$. Further, for $v > v_c$ the secondary maxima are attenuated much stronger than the main one. As a result, for a sufficiently large p only the main maximum survives for $v > v_c$.

Short account of the results obtained is given in sect. 8.

2 Mathematical preliminaries

Consider a point charge e uniformly moving in a non-magnetic medium with a velocity v directed along the z axis. Its charge and current densities are given by

$$\rho(\vec{r},t) = e\delta(x)\delta(y)\delta(z-vt), \quad j_z = v\rho.$$

Their Fourier transforms are

$$\rho(\vec{k},\omega) = \int \rho(\vec{r},t)\exp[i(\vec{k}\vec{r}-\omega t)]d^3\vec{r}dt = 2\pi e\delta(\omega - \vec{k}\vec{v}), \quad j_z(\vec{k},\omega) = v\rho(\vec{k},\omega).$$

In the $(\vec{k},\omega)$ space the electromagnetic potentials are given by (see, e.g., [18])

$$\Phi(\vec{k},\omega) = \frac{4\pi}{\epsilon}\frac{\rho(\vec{k},\omega)}{k^2 - \frac{\omega^2}{c^2}\epsilon}, \quad A_z(\vec{k},\omega) = 4\pi\beta\frac{\rho(\vec{k},\omega)}{k^2 - \frac{\omega^2}{c^2}\epsilon}, \quad \beta = v/c. \tag{2.1}$$

Here $\epsilon(\omega)$ is the electric permittivity of medium. In this section, its frequency dependence is chosen in a standard form (1.1). In the usual interpretation ω_L and ω_0 are the plasma frequency $\omega_L^2 = 4\pi N_e e^2/m$ (N_e is the number of electrons per unit of volume, m is the electron mass) and some resonance frequency. Quantum-mechanically, it can be associated with the energy excitation of the lowest atomic level. Our subsequent exposition does not depend on this particular interpretation of ω_L and ω_0. The static limit of $\epsilon(\omega)$ is $\epsilon_0 = \epsilon(\omega = 0) = 1 + \omega_L^2/\omega_0^2$. $\epsilon(\omega)$ has poles at $\omega = \pm\omega_0$. Being positive for $\omega^2 < \omega_0^2$ it jumps from $+\infty$ to $-\infty$ when one crosses the $\omega^2 = \omega_0^2$ point; $\epsilon(\omega)$ has zero at

$\omega^2 = \omega_0^2 + \omega_L^2$ and tends to unity as $\omega \to \infty$. Correspondingly.

$$\epsilon^{-1}(\omega) = 1 - \frac{\omega_L^2}{\omega_0^2 + \omega_L^2 - \omega^2} \tag{2.2}$$

has zero at $\omega^2 = \omega_0^2$ and a pole at $\omega^2 = \omega_3^2 = \omega_0^2 + \omega_L^2$. As it has been admitted in [10], the inclusion of ω dependencies in ϵ effectively takes into account the retardation effects. The very fact that the light velocity in medium c_n is less than the light velocity in vacuum c means that oscillators of medium react to the initial electromagnetic field with some delay (see section 5, for details). The deviation of c_n from c is due to the deviation of ϵ from unity. For the incoming plane wave and frequency-independent ϵ this was clearly demonstrated in refs. [19-21]. At first glance it seems that c_n will be greater than c for $\epsilon < 1$. However, a more accurate analysis shows [9] that the group velocity of light in medium is always less than c.

In the $\vec{r}, t$ representation $\Phi(\vec{r}, t)$ and $\vec{A}(\vec{r}, t)$ are given by

$$\Phi(\vec{r}, t) = \frac{e}{\pi v} \int \frac{d\omega}{\epsilon} e^{i\omega(t - z/v)} \frac{kdk}{k^2 + \frac{\omega^2}{v^2}(1 - \beta^2\epsilon)} J_0(k\rho),$$

$$A_z(\vec{r}, t) = \frac{e}{\pi c} \int d\omega e^{i\omega(t - z/v)} \frac{kdk}{k^2 + \frac{\omega^2}{v^2}(1 - \beta^2\epsilon)} J_0(k\rho). \tag{2.3}$$

First, we take integral over k. For this, we use the Table integral (see, e.g., [22])

$$\int_0^\infty \frac{kdk}{k^2 + q^2} J_0(k\rho) = K_0(\rho q), \tag{2.4}$$

where in the right-hand side the value of the square root $\sqrt{q^2}$ corresponding to its positive real part should be taken.

3 Electromagnetic potentials and field strengths

We write out nonvanishing components of the electromagnetic potential, field strength and induction:

$$\Phi = \frac{e}{\pi v} \int_{-\infty}^{\infty} \frac{d\omega}{\epsilon} e^{i\alpha} K_0(k\rho), \quad A_z = \frac{e}{\pi c} \int_{-\infty}^{\infty} d\omega e^{i\alpha} K_0(k\rho),$$

$$H_\phi = \beta D_\rho = \frac{e}{\pi c} \int_{-\infty}^{\infty} d\omega e^{i\alpha} k K_1(k\rho), \quad E_\rho = \frac{e}{\pi v} \int_{-\infty}^{\infty} \frac{d\omega}{\epsilon} e^{i\alpha} k K_1(k\rho),$$

$$E_z = -\frac{ie}{\pi c^2} \int_{-\infty}^{\infty} d\omega\omega(1 - \frac{1}{\beta^2\epsilon}) e^{i\alpha} K_0(k\rho), \quad D_z = \frac{ie}{\pi v^2} \int_{-\infty}^{\infty} d\omega\omega(1 - \beta^2\epsilon) e^{i\alpha} K_0(k\rho). \tag{3.1}$$

Here $\alpha = \omega(t - z/v)$, $k^2 = (1 - \beta^2\epsilon)\omega^2/v^2$. Again, k in Eq.(3.1) means the value of $\sqrt{k^2}$ corresponding to $Rek > 0$.

These expressions were obtained by Fermi [11]. Their drawback is that modified Bessel functions K are complex even for real ϵ (when $1 - \beta^2\epsilon < 0$). We now present Eqs. (3.1) in a manifestly real form. This greatly simplifies calculations.

At first, we define domains where $1 - \beta^2\epsilon > 0$ and $1 - \beta^2\epsilon < 0$.

For $\beta < \beta_c$ one has

$1 - \beta^2\epsilon > 0$ for $\omega^2 < \omega_c^2$ and $\omega^2 > \omega_0^2$ and $1 - \beta^2\epsilon < 0$ for $\omega_c^2 < \omega^2 < \omega_0^2$.

For $\beta > \beta_c$ one gets

$1 - \beta^2\epsilon > 0$ for $\omega^2 > \omega_0^2$ and $1 - \beta^2\epsilon < 0$ for $0 < \omega^2 < \omega_0^2$.

Here $\omega_c^2 = \omega_0^2(1 - \epsilon)$, $\epsilon = \beta^2\gamma^2/\beta_c^2\gamma_c^2$, $\beta_c^2 = 1/\epsilon_0$. In what follows we shall refer to β_c as to the light velocity in medium. It turns out that equations defining electromagnetic potentials and field strengths are essentially different for $\beta < \beta_c$ and $\beta > \beta_c$. For $\beta < \beta_c$ one gets [14]:

$$\Phi(\vec{r}, t) = \frac{2e}{\pi v}(\int_0^{\omega_c} + \int_{\omega_0}^{\infty}) \frac{d\omega}{\epsilon} \cos\alpha K_0 + \frac{e}{v} \int_{\omega_c}^{\omega_0} \frac{d\omega}{\epsilon} (\sin\alpha J_0 - \cos\alpha N_0),$$

$$A_z(\vec{r}, t) = \frac{2e}{\pi c}(\int_0^{\omega_c} + \int_{\omega_0}^{\infty}) d\omega \cos\alpha K_0 + \frac{e}{c} \int_{\omega_c}^{\omega_0} d\omega (\sin\alpha J_0 - \cos\alpha N_0) \tag{3.2}.$$

$$H_\phi(\vec{r}, t) = \frac{2e}{\pi c v}(\int_0^{\omega_c} + \int_{\omega_0}^{\infty}) \omega d\omega \sqrt{|1 - \beta^2\epsilon|} \cos\alpha K_1 + \frac{e}{cv} \int_{\omega_c}^{\omega_0} \omega d\omega \sqrt{|1 - \beta^2\epsilon|} (\sin\alpha J_1 - \cos\alpha N_1),$$

$$E_z = \frac{2e}{\pi c^2}(\int_0^{\omega_c} + \int_{\omega_0}^{\infty})(1 - \frac{1}{\epsilon\beta^2}) \omega d\omega \sin\alpha K_0 - \frac{e}{c^2} \int_{\omega_c}^{\omega_0} (1 - \frac{1}{\epsilon\beta^2}) \omega d\omega (N_0 \sin\alpha + J_0 \cos\alpha),$$

$$E_\rho = \frac{2e}{\pi v^2}(\int_0^{\omega_c} + \int_{\omega_0}^{\infty}) d\omega \frac{\omega}{\epsilon} \sqrt{|1 - \beta^2\epsilon|} \cos\alpha K_1 + \frac{e}{v^2} \int_{\omega_c}^{\omega_0} d\omega \frac{\omega}{\epsilon} \sqrt{|1 - \beta^2\epsilon|} (\sin\alpha J_1 - \cos\alpha N_1).$$

On the other hand, for $\beta > \beta_c$

$$\Phi(\vec{r}, t) = \frac{2e}{\pi v} \int_{\omega_0}^{\infty} \frac{d\omega}{\epsilon} \cos\alpha K_0 + \frac{e}{v} \int_0^{\omega_0} \frac{d\omega}{\epsilon} (\sin\alpha J_0 - \cos\alpha N_0),$$

$$A_z(\vec{r}, t) = \frac{2e}{\pi c} \int_{\omega_0}^{\infty} d\omega \cos\alpha K_0 + \frac{e}{c} \int_0^{\omega_0} d\omega (\sin\alpha J_0 - \cos\alpha N_0). \tag{3.3}$$

$$H_\phi(\vec{r}, t) = \frac{2e}{\pi c v} \int_{\omega_0}^{\infty} \omega d\omega \sqrt{|1 - \beta^2\epsilon|} \cos\alpha K_1 + \frac{e}{cv} \int_0^{\omega_0} \omega d\omega \sqrt{|1 - \beta^2\epsilon|} (\sin\alpha J_1 - \cos\alpha N_1),$$

$$E_z = \frac{2e}{\pi c^2} \int_{\omega_0}^{\infty} (1 - \frac{1}{\epsilon\beta^2}) \omega d\omega \sin\alpha K_0 - \frac{e}{c^2} \int_0^{\omega_0} (1 - \frac{1}{\epsilon\beta^2}) \omega d\omega (N_0 \sin\alpha + J_0 \cos\alpha),$$

$$E_\rho = \frac{2e}{\pi v^2}\int_{\omega_0}^{\infty} d\omega \frac{\omega}{\epsilon}\sqrt{|1-\beta^2\epsilon|}\cos\alpha K_1 + \frac{\epsilon}{v^2}\int_0^{\omega_0} d\omega\frac{\omega}{\epsilon}\sqrt{|1-\beta^2\epsilon|}(\sin\alpha J_1 - \cos\alpha N_1).$$

Here $\alpha = \omega(t - z/v)$. The argument of all the Bessel functions is $\sqrt{|1-\beta^2\epsilon|}\rho\omega/v$.
We observe that integrals containing usual (J, N) and modified (K) Bessel functions are taken over space regions where $1-\beta^2\epsilon < 0$ and $1-\beta^2\epsilon > 0$, resp. Obviously, there is no damping of the EMF radiated by a moving charge for $1-\beta^2\epsilon < 0$ and there is damping for $1-\beta^2\epsilon > 0$.
The Fourier components of Φ and $\vec{E}$ have a pole at $\omega^2 = \omega_3^2 = \omega_0^2 + \omega_L^2$. This leads to a divergence of the integrals defining Φ and $\vec{E}$. It turns out that only their non-divergent parts (containing non-modified Bessel functions J_μ and N_μ contribute to the radiation (see the next section). The divergent terms containing modified Bessel function K_μ describe the electromagnetic field carried by a moving charge. They become finite when the compex electric permittivity (1.2) is used (see sections 6 and 7).

4 The radiated energy flux

We evaluate now the energy flux per unit length through the surface of a cylinder C_ρ (Fig.1) coaxial with the z axis for the total time of motion. It is given by

$$W = \int_{-\infty}^{+\infty}\sigma_\rho dt = \frac{1}{v}\int_{-\infty}^{+\infty}\sigma_\rho dz,$$

$$\sigma_\rho = 2\pi\rho S_\rho, \quad S_\rho = \frac{c}{4\pi}(\vec{E}\times\vec{H})_\rho = -\frac{c}{4\pi}E_z H_\varphi. \tag{4.1}$$

Substituting here E_z and H_φ given by (3.2) and (3.3) and taking into account that

$$\int_{-\infty}^{\infty} dt\sin\omega t\cos\omega' t = 0, \quad \int_{-\infty}^{\infty} dt\sin\omega t\sin\omega' t = \pi[\delta(\omega-\omega') - \delta(\omega+\omega')],$$
$$\int_{-\infty}^{\infty} dt\cos\omega t\cos\omega' t = \pi[\delta(\omega-\omega') + \delta(\omega+\omega')],$$

we get for energy losses per unit length

$$W = \frac{e^2}{c^2}\int_{\beta^2\epsilon>1}\omega d\omega(1-\frac{1}{\epsilon\beta^2}). \tag{4.2}$$

This expression was obtained by Tamm and Frank [2]. Inserting into it $\epsilon(\omega)$ given by (1.1) we get

$$W = \frac{e^2}{c^2}\int_{\omega_c}^{\omega_0}\omega d\omega(1-\frac{1}{\epsilon\beta^2}) = -\frac{e^2\omega_0^2}{2c^2\beta_c^2\gamma_c^2}[1+\frac{1}{\beta^2}\ln(1-\beta^2)] \tag{4.3}$$

for $\beta < \beta_c$ and

$$W = \frac{e^2}{c^2}\int_0^{\omega_0}\omega d\omega(1-\frac{1}{\epsilon\beta^2}) = \frac{e^2\omega_0^2}{2c^2}[-\frac{1}{\beta^2\gamma^2} + \frac{1}{\beta^2\beta_c^2\gamma_c^2}\ln(\gamma_c^2)] \tag{4.4}$$

for $\beta > \beta_c$. Similar expressions were obtained by E. Fermi [11]. The validity of Eq.(4.2) is also confirmed by the results obtained by Sternheimer [23] (whose equations pass into (4.2) in the limit $p \to 0$) and Ginzburg [24].
We observe that only those terms in (3.2) and (3.3) which contain the usual Bessel functions (J_μ and N_μ) and correspond to $1-\beta^2\epsilon < 0$ region without damping contribute to the radial energy flux for the total motion time. This permits us to avoid troubles with the above-mentioned pole of ϵ^{-1} (at $\omega = \omega_3$) which appears only in terms containing modified Bessel functions in the damping region where $1-\beta^2\epsilon > 0$.

For $\beta \to 0$ the energy losses W tend to 0, while for $\beta \to 1$ (only this limit was considered by Tamm and Frank [2]) they tend to the finite value $\frac{e^2\omega_0^2}{2c^2\beta_c^2\gamma_c^2}\ln(\gamma_c^2)$.
In Fig. 2, we present the dimensionless quantity $F = W/(e^2\omega_0^2/c^2)$ as a function of the particle velocity β. The numbers at curves mean β_c. The vertical lines with arrows divide each curve into two parts corresponding to the energy losses with velocities $\beta < \beta_c$ and $\beta > \beta_c$ and lying to the left and right of vertical lines, resp. We see that the charge uniformly moving in medium radiates at every velocity.
Exactly the same Eqs. (4.2)-(4.4) are obtained if one starts from the complex $\epsilon(\omega)$ given by (1.2), evaluates electromagnetic strengths and radial energy flux and then takes the limit $p \to 0$ in them. This is done in section 7.

For frequency-independent electric permittivity ($\epsilon = \epsilon_0$) the energy flux is infinite on the surface of the Cherenkov-Mach cone. On the surface of C_ρ it acquires the infinite value at the place where C_ρ is intersected by the above cone. Inside the Mach cone the electromagnetic strengths fall as r^{-2} at large distances and, therefore, do not contribute to the radial flux.

The distributions of the radial energy flux $\sigma_\rho = 2\pi\rho S_\rho$ on the surface of the cylinder C_ρ of the radius $\rho = 10$ (in units c/ω_0) are shown in Figs. 3 and 4 for the value $\beta_c = 0.8$ and different charge velocities β. It is seen that despite the ω dependence of ϵ the critical velocity $\beta_c = 1/\sqrt{\epsilon_0}$ has still a physical meaning. Indeed, for $\beta > \beta_c$ the electromagnetic energy flux is very small outside the Mach cone exhibiting oscillations in its neighbourhood. For $\beta < \beta_c$ the radial flux diminishes and becomes negligible for $\beta \leq 0.4$ (Fig. 4). This disagrees with Fig. 2 where for $\beta_c = 0.8$ one sees the finite value of energy losses for $\beta = 0.4$. In the next section, we remove this inconsistency.
So far we considered the distribution of the EMF on the surface of C_ρ at the fixed moment of time t. Since all electromagnetic strengths depend on z and t via the combination $z - vt$, the periodic dependence of time should be observed at a fixed spatial point.

5 WKB estimates

For large values of ρ the radiation field (described by the integrals in (3.2) and (3.3) containing usual Bessel functions) can be handled by the WKB method. We closely follow Tamm's paper [25] (see also the review [26] and book [27]). The electromagnetic strengths and radial (i.e., in the ρ direction) energy flow have sharp maxima on some space surfaces. In the ρ, z coordinates these surfaces can be drawn (due to the axial symmetry of the problem) by the lines. We refer to them as to trajectories. Different trajectories are labelled by the integer numbers m. For the electric penetrability taken in the form (1.1), m runs from 1 to ∞. We make the notation $x_c^2 = 1 - \tilde{\epsilon}$, $\tilde{\epsilon} = \beta^2\gamma^2/\beta_c^2\gamma_c^2$. The trajectories can be parametrized by the equation

$$vt - z = \frac{m\pi c\beta}{\omega_0\tilde{\epsilon}x^3}[\tilde{\epsilon} - (x^2-1)^2], \quad \rho = \frac{m\pi c\beta\gamma}{\omega_0\tilde{\epsilon}x^3}(1-x^2)^{3/2}(x^2-x_c^2)^{1/2}. \qquad (5.1)$$

We consider cases $\beta > \beta_c$ and $\beta < \beta_c$ separately.

5.1 Charge velocity β exceeds critical velocity β_c

It turns out that $x_c^2 < 0$ for $\beta > \beta_c$. In this case x runs in the interval $0 < x < 1$. The particular trajectory begins at the point $x = 1$ where $vt - z = m\pi c/\omega_0$ and $\rho = 0$. The slope of the trajectory is

$$\tan\theta = \gamma\frac{(1-x^2)^{3/2}(x^2-x_c^2)^{1/2}}{\tilde{\epsilon} - (x^2-1)^2}.$$

When x decreases both $vt - z$ and ρ increase. For very small x

$$vt - z \sim \frac{m\pi c\beta}{\omega_0\tilde{\epsilon}x^3}(\tilde{\epsilon}-1), \quad \rho \sim \frac{m\pi c\beta\gamma}{\omega_0\tilde{\epsilon}x^3}\sqrt{\tilde{\epsilon}-1}.$$

The asymptotic slope of the trajectory is

$$\tan\theta = \frac{\rho}{vt-z} \sim (\frac{\beta^2}{\beta_c^2} - 1)^{-1/2}.$$

It is seen that the trajectory slope increases when β approaches β_c (Fig. 5).

Let $v = c$, i.e. the charge moves with the light velocity in vacuum. Then,

$$vt - z = \frac{m\pi c}{\omega_0 x^3}, \quad \rho = \frac{m\pi c}{x^3\omega_0}\beta_c\gamma_c(1-x^2)^{3/2}.$$

Eliminating x one gets

$$\rho = \beta_c\gamma_c(ct-z)[1 - (\frac{m\pi c}{\omega_0(ct-z)})^{2/3}]^{3/2}.$$

For large $ct - z$ the trajectory is linear: $\rho = \beta_c\gamma_c(ct - z)$. For $\beta_c \to 0$ the trajectory approaches the motion axis.

Let β be slightly greater than β_c:

$$\tilde{\epsilon} = 1 + \delta, \quad 0 < \delta << 1,$$

i.e., charge moves almost with the light velocity in medium. Then, in the limit $\delta \to 0$ one gets

$$vt - z = \frac{m\pi v}{\omega_0 x}(2 - x^2), \quad \rho = \frac{m\pi v\gamma}{\omega_0 x^2}(1-x^2)^{3/2}. \qquad (5.2)$$

Excluding x we obtain

$$\rho = \frac{m\pi c\beta_c\gamma_c}{\omega_0}\frac{[y\sqrt{2+y^2/4} - 1 - y^2/2]^{3/2}}{y^2 + 2 - y\sqrt{2+y^2/4}}.$$

Here $y = \omega_0(vt - z)/m\pi c\beta_c$. At large distances one has:

$$\rho \sim \frac{\omega_0\gamma_c}{4m\pi c\beta_c}(vt-z)^2.$$

That is, ρ increases quadratically with the rise of $vt - z$.

5.2 Charge velocity β is less than the critical velocity β_c

For $\beta < \beta_c$ one has $\tilde{\epsilon} < 1$ and $x_c^2 > 0$. The trajectory parametrization coincides with (5.1) when x is in interval $\sqrt{4-3\tilde{\epsilon}} - 1 < x^2 < 1$. We refer to this part of trajectory as to branch 1. For $\beta < \beta_c$ and $1 - \tilde{\epsilon} < x^2 < \sqrt{4-3\tilde{\epsilon}} - 1$ the parametrization is given by Eq.(5.1) in which m should be changed by $m - 1/2$. This part of trajectory is denoted as branch 2. These branches are marked by numbers 1 and 2 in Fig. 6. It is seen that ρ vanishes for $x = x_c$ and $x = 1$. The corresponding $vt - z$ lie on the branches 1 and 2, respectively. As the values of $vt - z$ for which $\rho = 0$ are finite, the trajectories are closed for $\beta < \beta_c$.

Let β be slightly less than β_c, that is

$$\tilde{\epsilon} = 1 - \delta, \quad 0 < \delta << 1,$$

i.e., charge moves with the velocity slightly lesser than the light velocity in medium. Then, parametrizations of $vt - z$ and ρ are still given by (5.2) in which x changes in the interval $3\delta/2 < x^2 < 1$ for the first branch and in the interval $\delta/2 < x^2 < 3\delta/2$ for the second branch. This means that the first branch of the m trajectory for $\beta = \beta_c - \delta$ continuously passes into the corresponding m trajectory for $\beta = \beta_c + \delta$, .. $\delta \to 0$.
As to the second branch, in the limit $\delta \to 0$ it degenerates into the almost vertical line. It begins at $z = (m - 1/2)\pi c\beta/\omega_0\sqrt{\delta}$ where $\rho = 0$ and terminates at $z = (m - 1/2)\pi c\beta 4\sqrt{2}/(3\sqrt{3}\omega_0\sqrt{\delta})$ where $\rho = 2(m - 1/2)\pi c\beta\gamma/(3\sqrt{3}\omega_0\delta)$ (see Fig.6).

Let $\tilde{\epsilon} \to 0$. This may happen when the charge velocity is much less than the light velocity in medium. However, this condition may be also fulfilled when $\beta \approx \beta_c \approx 1$, but

β_c is much closer to 1 than β. This is possible because of the γ factors in the definition of $\tilde{\epsilon}$. In both cases one has

$$vt - z \to \frac{m\pi v}{\omega_0}, \quad \rho \to 0.$$

This means that radiation flux is concentrated behind the charge on the motion axis.

The WKB approximation breaks at the neighbourhood of $x = x_m = (\sqrt{4-3\tilde{\epsilon}}-1)^{1/2}$. This value can be reached only for $\beta < \beta_c$. The values of z and ρ at those points are

$$(vt-z)_1 \sim \frac{4m\pi c\beta}{\omega_0\tilde{\epsilon}} \frac{\tilde{\epsilon}+\sqrt{4-3\tilde{\epsilon}}-2}{(\sqrt{4-3\tilde{\epsilon}}-1)^{3/2}},$$

$$\rho_1 \sim \frac{m\pi c\beta\gamma}{\omega_0\tilde{\epsilon}} \frac{(\tilde{\epsilon}+\sqrt{4-3\tilde{\epsilon}}-2)^{1/2}(2-\sqrt{4-3\tilde{\epsilon}})^{3/2}}{(\sqrt{4-3\tilde{\epsilon}}-1)^{3/2}}$$

for the branch 1. For the branch 2, m should be changed by $m - 1/2$. The slope of the line C_m (strictly speaking, it is a cone rather than the line, but in the (ρ, z) plane it looks like a line (Figs. 7 and 8)) passing through the discontinuity points is given by

$$\tan\theta = \frac{\gamma}{4} \frac{(2-\sqrt{4-3\tilde{\epsilon}})^{3/2}}{(\sqrt{4-3\tilde{\epsilon}}+\tilde{\epsilon}-2)^{1/2}}.$$

In particular,

$$\tan\theta \sim \frac{3\sqrt{3}}{16}\gamma\tilde{\epsilon} \quad \text{for} \quad \tilde{\epsilon} \to 0 \quad \text{and}$$

$$\tan\theta \sim \frac{1}{2\sqrt{2}} \frac{\gamma}{\sqrt{\delta}} \quad \text{for} \quad \tilde{\epsilon} \to 1 \quad (\tilde{\epsilon} = 1-\delta, \quad \delta << 1).$$

That is, the slope of C_m line tends to zero for small charge velocity and becomes large as β approaches β_c. The meaning of this line that on a particular trajectory (which itself is the line where field strengths are maximal) the field strengths become infinite as one approaches the point at which the WKB method breaks.

On the surface of the cylinder C_ρ (see Fig.1) the field strengths have maxima at those points where C_ρ is intersected by the trajectories. Among these maxima the most pronounced (i.e., of the greatest amplitude) are expected to be those which lie near the point at which C_ρ is intersected by C_m (despite the WKB approximation breaking on it). In what follows we shall use this fact as a tool for the rough estimation of the position where the radiation intensity is maximal. This will be confirmed by exact calculations).

Some of the trajectories corresponding to $\beta_c = 0.8$, $\beta = 0.4$ are shown in Figs. 7 and 8. It follows from them that there are no trajectories intersecting the surface of the cylinder C_ρ of the radius $\rho = 10$ in the interval $-100 < z < 0$ treated in Fig. 4. This means that there should be no radial energy flux there. The inspection of Fig. 8 tells us that for $\rho = 10$ the energy flux begins to penetrate the C_ρ surface at the distances $z \le -200$.

6 Numerical results

To verify WKB estimates we evaluated the distribution of the energy losses σ_ρ on the surface of C_ρ (Fig. 9). It is seen that the main contribution comes from the region in the neighbourhood $z \sim -300$. This σ_ρ distribution consists, in fact, of many peaks. Its fine structure in the small z interval is shown in Fig. 10.

The question arises how the trajectories behave for other charge velocities β. It follows from Fig. 5 that for $\beta \ge \beta_c$ the trajectories are not closed, i.e. they go to infinity as z tends to $-\infty$. The slope of the trajectories increases as β approaches β_c. This reflects the fact that for $\beta = \beta_c$ EMF of the charge moving uniformly in non-dispersive medium differs from zero only in the infinitely thin layer normal to the charge velocity [6]. Since for $\beta > \beta_c$ the trajectories intersect the C_ρ surface at small values of z, one should expect the appearance of the energy flux there. In Figs. 11 and 12 we present the results of exact (i.e., not WKB) calculations of the intensity distribution for $\beta = 0.99$ and 0.8, resp. We observe that for $\beta > \beta_c$ the main intensity maximum lies approximately at $z = -z_c$, $z_c = \rho\sqrt{\frac{\beta^2}{\beta_c^2}-1}$, i.e., at the place where in the absence of the ω dispersion ($\epsilon = \epsilon_0 = \epsilon(0)$, $\beta_c^2 = 1/\epsilon_0$) the Cherenkov singular cone intersects C_ρ.

For $\beta < \beta_c$ the trajectories are closed (Figs. 6, 7, 8 and 13). As β decreases, the trajectories approach the motion axis. In this case, the C_ρ surface is intersected by the trajectories with large m at larger negative z values (compared to the $\beta > \beta_c$ case) and the intensity maxima should also be shifted to the large negative z. This is illustrated by Figs. 9 and 14 where the intensity spectra are shown for $\beta = 0.4$ and 0.6, resp.

Consider now the distribution of the radiation flux on the surface of the sphere S (instead on the cylinder surface, as we have done up to now). From Figs. 7 and 8 based on the WKB estimates and numerical results presented in Fig. 9 it follows that for $\beta < \beta_c$ the radial radiation flux is confined to the narrow cone adjusted to the negative z semi-axis (Fig. 15). Its solution angle θ_c equals approximately 5 degrees for $\beta_c = 0.8$ and $\beta = 0.4$. This gives a clue for the explanation of experiments discussed in [15-17]. In them, for the electron moving in a gas with a fixed energy the radiation intensity was measured as a function of the gas pressure. The gas pressure P is related to its density N_g by the well-known thermodynamic relation : $PV = kN_gT$, where V is the fixed gas volume, T its temperature and k is the Boltzmann constant. The quantities N_e, ω_L^2 and β_c used in section 2 are connected with N_g as follows:

$$N_e = N_g \cdot Z, \quad \omega_L^2 = 4\pi N_e c^2/m, \quad \beta_c^2 = \frac{\omega_0^2}{\omega_0^2+\omega_L^2}.$$

Here Z is the atomic number of gas. Let the gas pressure, at which $\beta_c = \beta$, be equal to p_c. In the experiments quoted above a sharp reduction of the radiation intensity was observed for the gas pressure $p \approx p_c/100$. To this pressure corresponds $\tilde{\epsilon} << 1$ despite

the fact that $\beta \approx \beta_c \approx 1$ (this is possible because of the γ factors in the definition of $\tilde{\epsilon}$). We associate this reduction with the narrowing of the radiation cone (see Fig. 15).
We conclude that despite the ω dependence of ϵ, the critical velocity $\beta_c = 1/\sqrt{\epsilon_0}$ still conserves its physical meaning, thus, separating closed ($\beta < \beta_c$) and unclosed ($\beta > \beta_c$) trajectories.

6.1 Estimation of non-radiation terms.

Up to now, when evaluating σ_ρ we have taken into account only those terms in $\vec{E}$ and $\vec{H}$ which contribute to the energy losses, i.e., to the W given by Eq. (4.1). They correspond to the terms of $\vec{E}$ and $\vec{H}$ containing the usual (non-modified) Bessel functions (see Eqs. (3.2) and (3.3)). However, we cannot use Eqs.(3.2) and (3.3) to evaluate terms with modified Bessel functions as their contribution to $\vec{E}$ is divergent. Instead, the following trick is used. We find $\vec{E}$ and $\vec{H}$ for the complex electric permittivity (1.2). They are finite for the non-zero value of parameter p defining the imaginary part of $\epsilon(\omega)$. The corresponding formulae are collected in section 7. Then, we tend the parameter p defining the imaginary part of ϵ to zero. We expect that for sufficiently small p we get the values of $\vec{E}$ and $\vec{H}$ which adequately describe the contribution of the terms with modified Bessel functions. There is another approach [28] in which the electric strength $\vec{E}$ is not singular (except for the charge motion axis) even for real ϵ. It turns out that electromagnetic strengths evaluated according to the formulae of section 7 are indistinguishable from those of Ref. [27] when the parameter p is of an order of $10^{-5} - 10^{-4}$ in units ω_0. In what follows, by the words " terms with modified Bessel functions are taken into account" we mean that the calculations are made by means of formulae presented in section 7 for $p = 10^{-4}$.

When the terms with modified Bessel functions are taken into consideration, the characteristic oscillation of σ_ρ appears in the neigbourhood $z = 0$ (Figs. 16 and 17). Approximately, for $\beta < \beta_c$ it is described by the following expression:

$$\sigma_\rho^1 = -\frac{c\beta e^2}{2\epsilon_0}(1 - \beta^2/\beta_c^2)^2 \frac{\rho^2 z}{[z^2 + \rho^2(1 - \beta^2/\beta_c^2)]^3} \qquad (6.1)$$

corresponding to the energy flux carried by the uniformly moving charge with the velocity $\beta < \beta_c$ in medium with a constant $\epsilon = \epsilon_0$. As we have mentioned, the terms in (3.2) and (3.3) containing modified Bessel functions do not contribute to the total energy losses (4.2). In particular, this is valid for σ_ρ^1 given by (6.1):

$$\int_{-\infty}^{\infty} \sigma_\rho^1 dz = 0$$

(due to the antisymmetry of σ_ρ). For $z >> \rho$ and $\rho >> z$, σ_ρ^1 falls as ρ^2/z^5 and z/ρ^4, resp. For $\beta = 0.4$ we estimate the value of the term (6.1) in the region $z = -300$ where σ_ρ has

maximum (see Fig. 9). It turns out that $\sigma_\rho \approx 6 \cdot 10^{-5}$ and $\sigma_\rho^1 \approx 5 \cdot 10^{-12}$ there, i.e., the contribution of σ_ρ^1 relative to σ_ρ is of an order of 10^{-7} and, therefore, it is negligible.
For $\beta = 0.6$ we see in Fig. 14 the σ_ρ distribution evaluated via Eqs. (3.2) and (3.3) in which the terms with modified Bessel functions are omitted. Comparing Fig. 9 with 16 and Fig. 14 with 17 we conclude that they coincide everywhere except for the $z = 0$ region where the term (6.1) is essential.
For $\beta \geq \beta_c$ the contribution of the terms involving modified Bessel functions in (3.2) and (3.3) is very small. This illustrates Fig. 18 where two distributions σ_ρ with and without inclusion of the above-mentioned terms are shown for $\beta = 0.8$. They are indistinguishable on this figure and look like one curve. The same is valid for larger charge velocities.

7 The influence of the imaginary part of ϵ

So far, we evaluated the total energy losses per unit length (W) and their distribution along the z axis (σ_ρ) for the pure real electric permittivity given by (1.1). Equation (1.2) is a standard parametrization of the complex electric permittivity ([29, 30]). For the chosen definition (2.3) of the Fourier transform the causality principle requires p to be positive.

We write out electromagnetic potentials and field strengths for the finite value of a parameter p defining the imaginary part of ϵ. Since $\epsilon(-\omega) = \epsilon^*(\omega)$, the EMF can be written in a manifestly real form

$$\Phi = \frac{2e}{\pi v}\int_0^\infty [(\epsilon_r^{-1}\cos\alpha - \epsilon_i^{-1}\sin\alpha)K_{0r} - (\epsilon_i^{-1}\cos\alpha + \epsilon_r^{-1}\sin\alpha)K_{0i}]d\omega,$$

$$A_z = \frac{2e}{\pi c}\int_0^\infty d\omega(\cos\alpha K_{0r} - \sin\alpha K_{0i}),$$

$$H_\phi = \frac{2e}{\pi v c}\int_0^\infty \omega d\omega (a^2+b^2)^{1/4}[\cos(\frac{\phi}{2}+\alpha)K_{1r} - \sin(\frac{\phi}{2}+\alpha)K_{1i}],$$

$$E_z = -\frac{2}{\pi v^2}\int_0^\infty \omega d\omega\{[\cos\alpha(\epsilon_r^{-1} - \beta^2) - \sin\alpha\epsilon_i^{-1}]K_{0i} + [\sin\alpha(\epsilon_r^{-1} - \beta^2) + \cos\alpha\epsilon_i^{-1}]K_{0r}\},$$

$$E_\rho = \frac{2}{\pi v^2}\int_0^\infty \omega d\omega (a^2+b^2)^{1/4}[(\epsilon_r^{-1}\cos\alpha - \epsilon_i^{-1}\sin\alpha)(\cos\frac{\phi}{2}K_{1r} - \sin\frac{\phi}{2}K_{1i}) -$$

$$-(\epsilon_i^{-1}\cos\alpha + \epsilon_r^{-1}\sin\alpha)(\sin\frac{\phi}{2}K_{1r} + \cos\frac{\phi}{2}K_{1i})]. \qquad (7.1)$$

Here we put

$$K_{0r} = ReK_0(\frac{\rho\omega}{v}\sqrt{1-\beta^2\epsilon}), \quad K_{0i} = ImK_0(\frac{\rho\omega}{v}\sqrt{1-\beta^2\epsilon}),$$

$$K_{1r} = ReK_1(\frac{\rho\omega}{v}\sqrt{1-\beta^2\epsilon}), \quad K_{1i} = ImK_1(\frac{\rho\omega}{v}\sqrt{1-\beta^2\epsilon}).$$

Further, ϵ_r and ϵ_i are the real and imaginary parts of ω

$$\epsilon_r = 1 + \frac{\omega_L^2(\omega_0^2-\omega^2)}{(\omega_0^2-\omega^2)^2+p^2\omega^2}, \quad \epsilon_i = -\frac{p\omega\omega_L^2}{(\omega_0^2-\omega^2)^2+p^2\omega^2},$$

$\epsilon_r^{-1} = \epsilon_r/(\epsilon_r^2+\epsilon_i^2)$, $\epsilon_i^{-1} = -\epsilon_i/(\epsilon_r^2+\epsilon_i^2)$; $\alpha = \omega(t-z/v)$;

$$a = 1-\beta^2-\beta^2\omega_L^2\frac{\omega_0^2-\omega^2}{(\omega_0^2-\omega^2)^2+p^2\omega^2}, \quad b = \beta^2\omega_L^2\frac{\omega p}{(\omega_0^2-\omega^2)^2+p^2\omega^2},$$

$$\cos\frac{\phi}{2} = \frac{1}{\sqrt{2}}(1+\frac{a}{\sqrt{a^2+b^2}})^{1/2}, \quad \sin\frac{\phi}{2} = \frac{1}{\sqrt{2}}\frac{b}{|b|}(1-\frac{a}{\sqrt{a^2+b^2}})^{1/2}.$$

The energy flux per unit length through the surface of a cylinder of the radius ρ coaxial with the z axis for the whole time of charge motion is defined by Eq.(4.1). Substituting E_z and H_ϕ given by (7.1) into it one gets

$$W = \int_0^\infty f(\omega)d\omega,$$

where

$$f(\omega) = -\frac{2e^2\rho}{\pi v^3}\omega^2(a^2+b^2)^{1/4}\{(K_{0r}K_{1r}+K_{0i}K_{1i})[(\epsilon_r^{-1}-\beta^2)\sin\frac{\phi}{2}-\epsilon_i^{-1}\cos\frac{\phi}{2}]-$$

$$-(K_{0i}K_{1r}-K_{0r}K_{1i})[(\epsilon_r^{-1}-\beta^2)\cos\frac{\phi}{2}+\epsilon_i^{-1}\sin\frac{\phi}{2}]\}. \qquad (7.2)$$

Consider now the limit $p \to 0$.

Let $1-\beta^2\epsilon > 0$ in this limit, then (see section 3):

$$\sin\frac{\phi}{2} \to 0,\ \cos\frac{\phi}{2} \to 1,\ \epsilon_i \to 0,\ \epsilon_i^{-1} \to 0,\ K_{0i} \to 0,\ K_{1i} \to 0$$

and, therefore, $f(\omega) \to 0$ while electromagnetic potentials and field strengths coincide with those terms in (3.2) and (3.3) which contain modified Bessel functions.

On the other hand, if in this limit $1-\beta^2\epsilon < 0$, then:

$$\sin\frac{\phi}{2} \to 1 \text{ (for } p>0),\ \cos\frac{\phi}{2} \to 0,\ \epsilon_i \to 0,\ \epsilon_i^{-1} \to 0,$$

$$K_{0r} \to -\frac{\pi}{2}N_0,\ K_{0i} \to -\frac{\pi}{2}J_0,\ K_{1r} \to -\frac{\pi}{2}J_1,\ K_{1i} \to \frac{\pi}{2}N_1,$$

where the argument of the Bessel functions is $\rho\frac{|\omega|}{v}\sqrt{|1-\beta^2\epsilon|}$. Substituting this into (7.2) and using the relation

$$J_\nu(x)N_{\nu+1}(x) - N_\nu(x)J_{\nu+1}(x) = -\frac{2}{\pi x}$$

one arrives at

$$f(\omega) = \frac{e^2\omega}{c^2}(1-\frac{1}{\epsilon\beta^2}).$$

This in turn leads to W exactly coinciding with (4.2),(4.3) and (4.4). Electromagnetic potentials and field strengths (7.1) coincide with the terms in (3.2) and (3.3) containing usual Bessel functions.

Now we intend to clarify how the value of the parameter p affects on the radiated electromagnetic field. For this we evaluated σ_ρ for $\beta = 0.4$ on the surface of cylinder C_ρ. $\rho = 10$ for three different values of parameter p (in units ω_0): $p = 10^{-3}$ (Fig. 19), $p = 10^{-2}$ and $p = 0.1$ (Fig. 20). We observe that for $p = 10^{-3}$ the intensity amplitude is approximately twice times less than for $p = 10^{-4}$ (Fig. 16). For $p = 10^{-2}$ and $p = 0.1$ all oscillations of σ_ρ on the negative z semi-axis are washed out while the value of the term corresponding to the modified Bessel functions in (3.2) and (3.3) remains almost the same. In Figs. 21 and 22 there are given distributions of the radiated energy on the surface of σ_ρ for $\beta = 0.8$ and $\beta = 0.99$ for three different values of $p = 10^{-3}$, 0.1 and 1. We note that with a rise of p the oscillations for $\beta < \beta_c$ are damped much stronger than for $\beta \geq \beta_c$. For example, for $p = 10^{-2}$ and $\beta = 0.99$ the values of the main maxima only slightly reduce (Fig. 22) while for $\beta = 0.4$ and the same p the oscillations of the radiation intensity completely disappear (Fig. 20).

Another observation is that secondary maxima are damped much stronger than the main one. This is easily realized within the polarization formalism. In it, a moving charge creates a time-dependent polarization source which, in the absence of damping, oscillates with the frequency $\sqrt{\omega_0^2+\omega_L^2}$. The oscillating polarization results in the appearance of secondary electromagnetic waves which being added are manifested as maxima of the potentials, field strengths, and intensities. The distribution of the polarization source for the electric permittivity (1.2) is given by [14]

$$div\vec{P} = \frac{e}{v}\delta(x)\delta(y)\frac{\omega_L^2}{\sqrt{\omega_0^2+\omega_L^2-p^2/4}}\exp[-p(t-z/v)/2]\cdot\sin[\sqrt{\omega_0^2+\omega_L^2-p^2/4}(t-z/v)] \qquad (7.3)$$

for $z < vt$ and $div\vec{P} = 0$ for $z > vt$ (this equation is related to the $\omega_0^2+\omega_L^2-p^2/4 > 0$ case). As a result of positivity of p, the value of polarization $\vec{P}$ at the moment t is defined by the values of the electric field $\vec{E}$ in preceeding times (causality principle). It follows from (7.3) that for large negative values of z the polarization source is suppressed much stronger than for z values close to the current charge position.

The position of the first maximum approximately coincides with the position of the singular Mach cone in the absence of dispersion.

Although the polarization formalism leads to the same expressions (3.2),(3.3) for the electromagnetic potentials and field strengths, it presents another, more physical, point of view on the nature of the Vavilov-Cherenkov radiation.

The total energy losses per unit length W (in units $e^2\omega_0^2/c^2$) and the total number of emitted photons N (in units $e^2\omega_0/\hbar c^2$) as a function of charge velocity $\beta = v/c$ for $\beta_c = 0.8$ and different values of p are shown in Figs. 23 and 24. In most the cases W and N decrease with the rising of p. The sole exception the origin of which remains unclear for us is the intersection of $N(\beta)$ curves corresponding to $p = 0.1$ and $p = 1$ (Fig. 24). The corresponding ω densities ($W = \int f(\omega)d\omega$ and $N = \int n(\omega)d\omega$) are shown in Figs. 25 and 26.

8 Conclusion

We briefly summarize the main results obtained:

1. We confirm the famous Fermi's result that a charge uniformly moving in medium with frequency-dependent polarizations (1.1) and (1.2) radiates at each velocity. We prove that ω dispersion of ϵ results in a rather complicated space distribution of EMF. In particular, the distribution of the radiation exhibits rapid oscillations behind the moving charge which differ drastically below and above some critical charge velocity v_c which depends on medium properies and does not depend on the frequency. For $v < v_c$ the major contribution to the radiation flux comes from the distant region of space lying behind the moving charge. The mathematical reason for this is that lines of maximal radiation intensity are closed for $v < v_c$ and unclosed for $v > v_c$.
2. We analyze how the imaginary part of dielectric permittivity affects the space distribution of the energy radiated by the uniformly moving charge. It turns out that the switching on the imaginary part of ϵ results in a considerable reduction of the intensity radiation for $v < v_c$ and in the attenuation of secondary maxima of the radiation intensity for $v > v_c$.

We believe that results obtained in this paper may be useful for the analysis of the experiments recently discussed in [15-17].

Acknowledgments

The authors would like to thank Prof. A.A. Tyapkin and Prof. V.P. Zrelov for useful discussions.

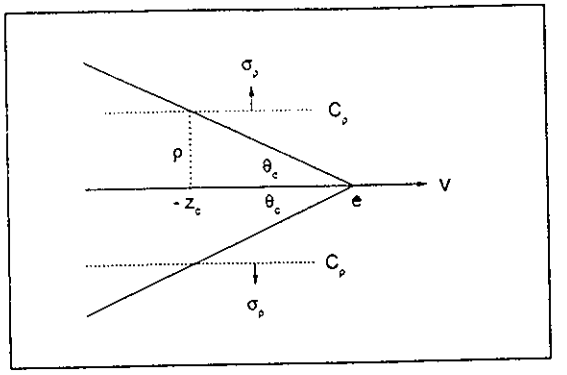

Figure 1: Schematic presentation of the Cherenkov cone for a constant electric permittivity. The radiation field is confined to the surface of the cone, the field inside the cone does not contribute to the radiation. On the surface of the cylinder C_ρ the electromagnetic field is zero for $z > -z_c$ and infinite at $z = -z_c$; σ_ρ means the radial energy flux through the cylinder surface.

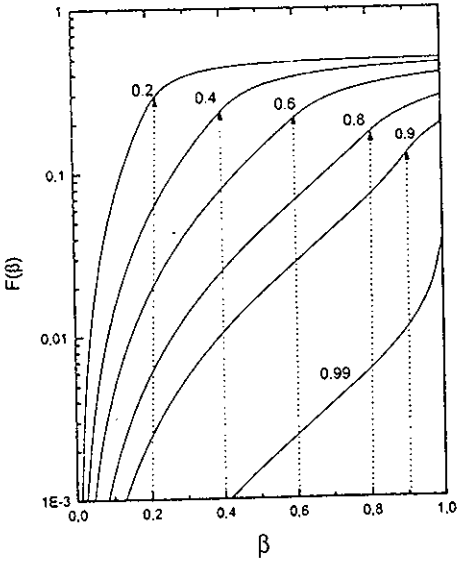

Figure 2: The radial energy losses per unit length (in units $e^2\omega_0^2/c^2$) as a function of $\beta = v/c$. The number of a particular curve means the critical velocity β_c.

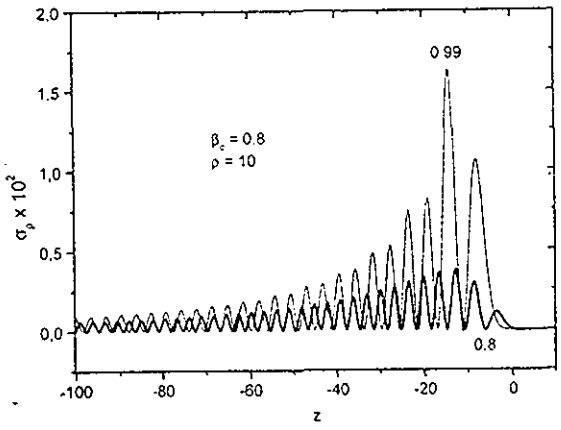

Figure 3: The distribution of the radial energy flux (in units $e^2\omega_0^3/c^3$) on the surface of the cylinder C_ρ, z is in units c/ω_0. The number of a particular curve means $\beta = v/c$.

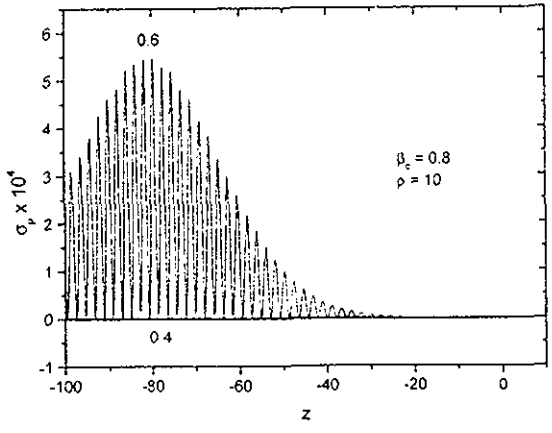

Figure 4: The same as in Fig.3, but for $\beta < \beta_c$.

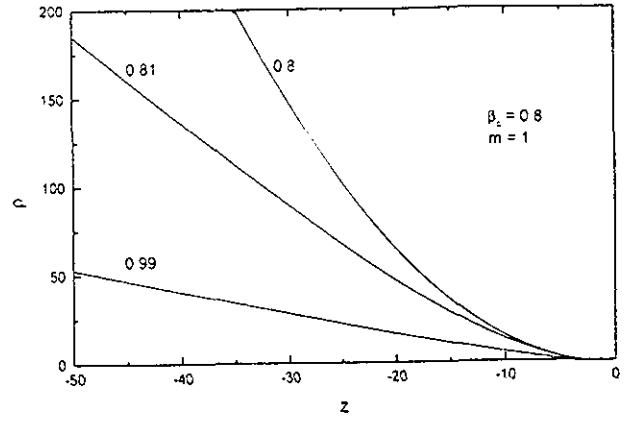

Figure 5: Space distribution of the $m = 1$ trajectory for charge velocities $\beta \geq \beta_c$. The slope of the trajectory increases as β approaches β_c.

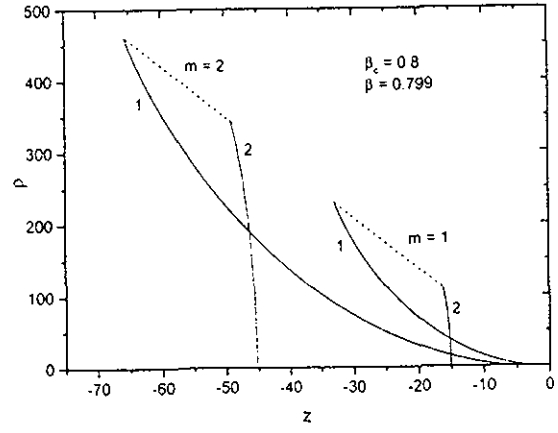

Figure 6: Space distribution of the $m = 1$ and $m = 2$ trajectories for $\beta_c = 0.8$ and $\beta = 0.799$. The trajectories for $\beta < \beta_c$ are closed (in contrast with the $\beta \geq \beta_c$ case shown in Fig. 5). Numbers 1 and 2 mean the branches of a particular trajectory.

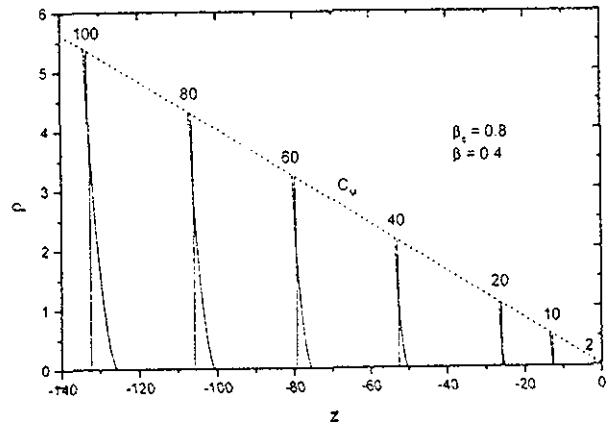

Figure 7: Space distribution of the selected trajectories for $\beta_c = 0.8$ and $\beta = 0.4$.

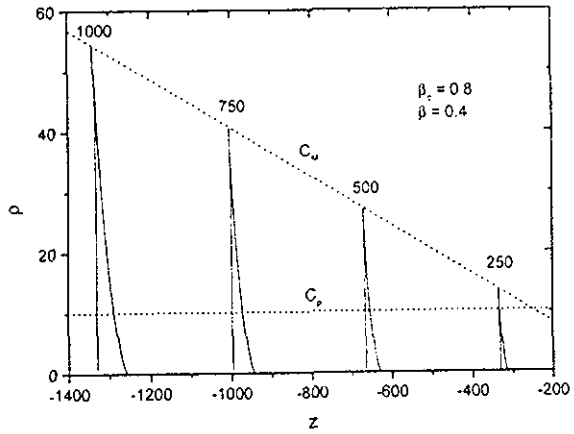

Figure 8: The same as in Fig. 7 but for the different z interval.

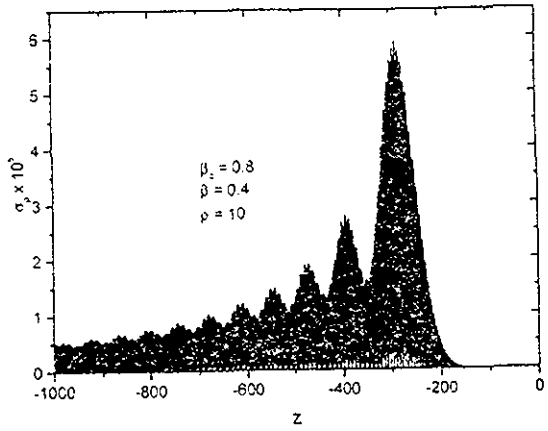

Figure 9: The distribution of the radial energy flux (in units $e^2\omega_0^3/c^3$) on the surface of the cylinder C_ρ for $\beta = 0.4$; z is in units c/ω_0. It is seen that the main contribution comes from large negative z.

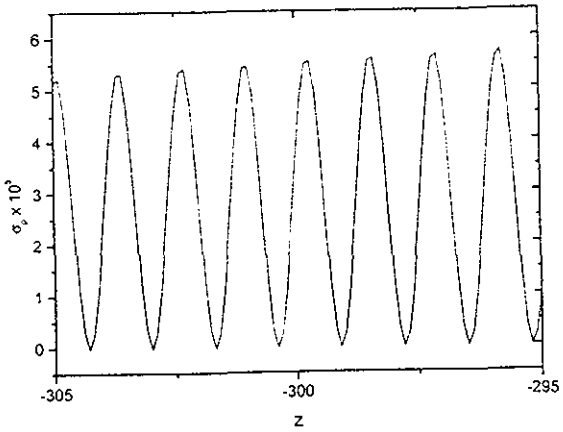

Figure 10: Fine structure of the radial energy flux shown in Fig. 9.

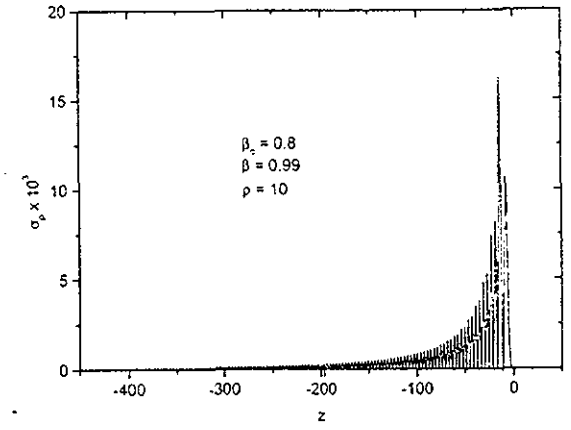

Figure 11: The distribution of the radial energy flux (in units $e^2\omega_0^3/c^3$) on the surface of the cylinder C_ρ for $\beta_c = 0.99$: z is in units c/ω_0 It is seen that the main contribution comes from the small negative values of z.

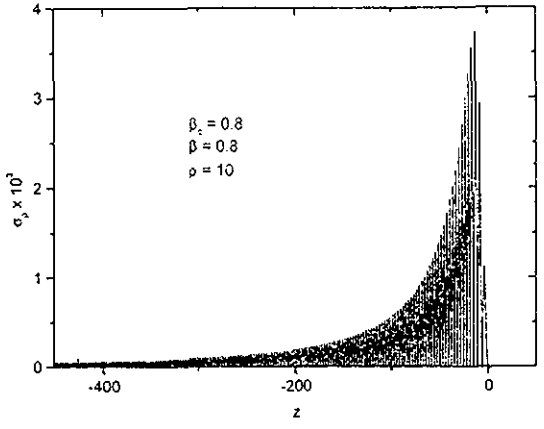

Figure 12: The same as in Fig. 11 but for $\beta = 0.8$. The radial energy flux is distributed in a greater z interval.

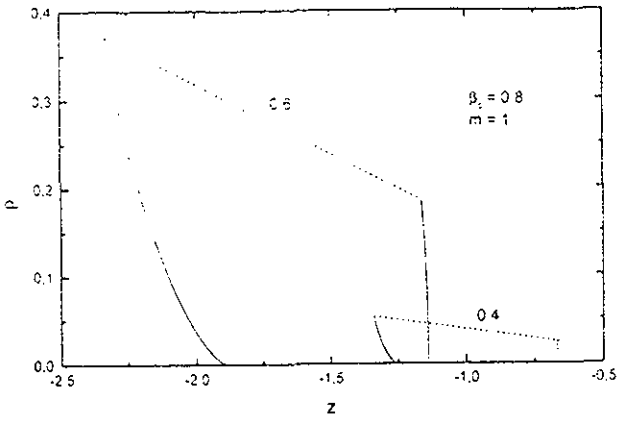

Figure 13: The behaviour of the $m = 1$ trajectory for $\beta = 0.4$ and $\beta = 0.6$. For $\beta < \beta_c$ the trajectories are grouped near the z axis. This shifts the maximum of the energy flux distribution to larger negative z.

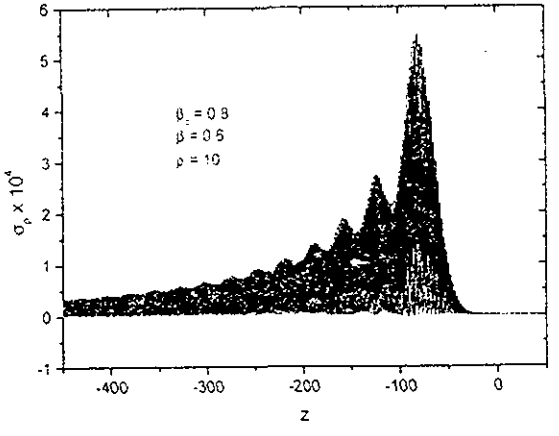

Figure 14: The same as in Fig. 7, but for the charge velocity $\beta = 0.6$.

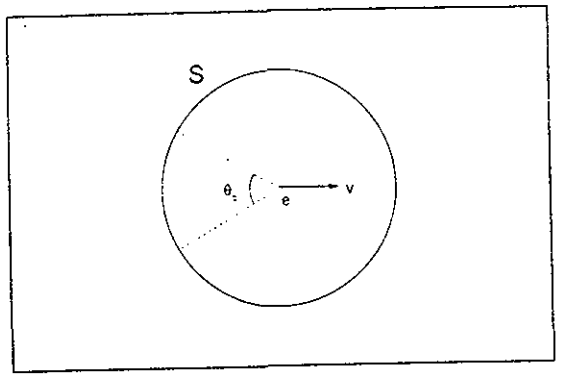

Figure 15: For the charge velocity β below some critical β_c the radial energy flux is confined to the narrow cone attached to the moving charge. For $\beta_c = 0.8$ and $\beta = 0.4$ the solution angle $\theta_c \approx 5°$.

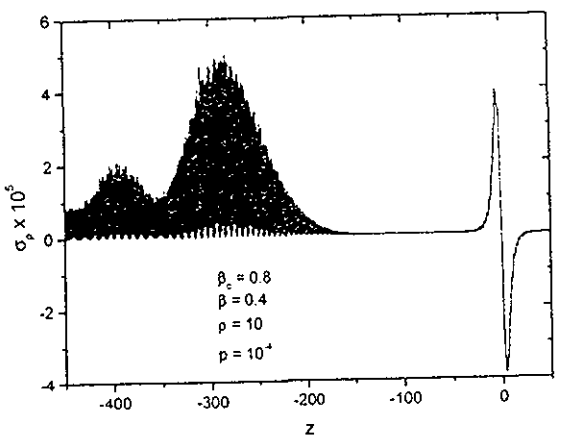

Figure 16: The same as in Fig. 7, but with the inclusion of the non-radiating term corresponding to the electromagnetic field carried by a moving charge.

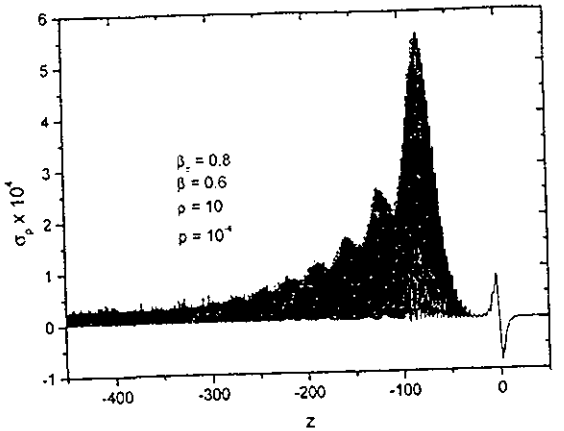

Figure 17: The same as in Fig. 16, but for the charge velocity $\beta = 0.6$.

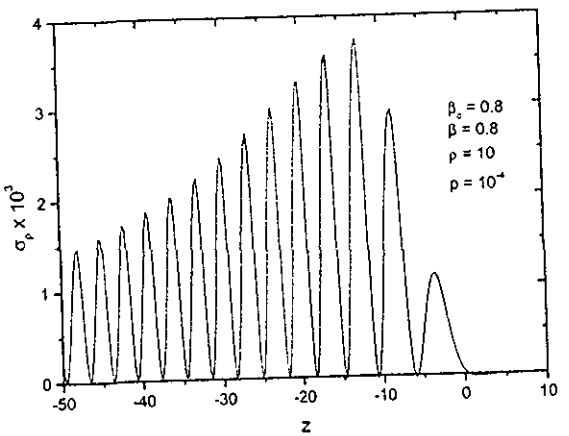

Figure 18: For $\beta = \beta_c$ the energy flux distributions with and without non-radiating term are practically the same: they are indistinguishable on this figure. The same is hold for $\beta > \beta_c$.

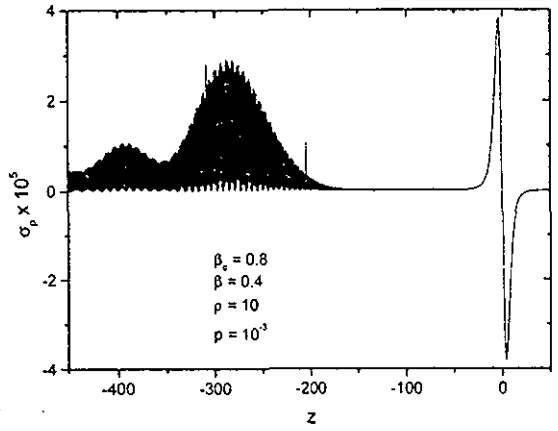

Figure 19: The switching on the imaginary part of ϵ ($p = 10^{-3}$) reduces the oscillation amplitude approximately by a factor of 2 compared to that for $p = 10^{-4}$ (see Fig. 16). The non-radiating term is practically the same as in Fig. 16.

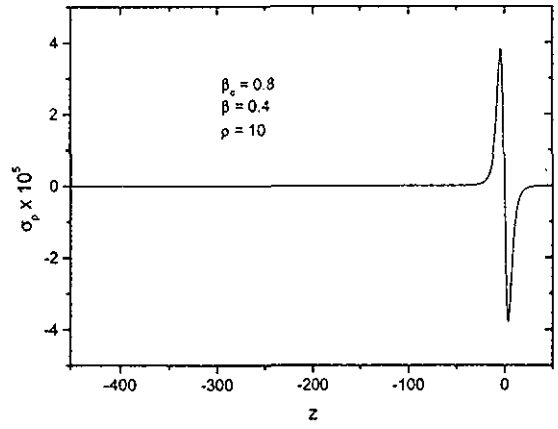

Figure 20: The radial energy flux for $p = 10^{-2}$ and $p = 10^{-1}$. The oscillations completely disappeared, but the value of the non-radiating term remains practically the same.

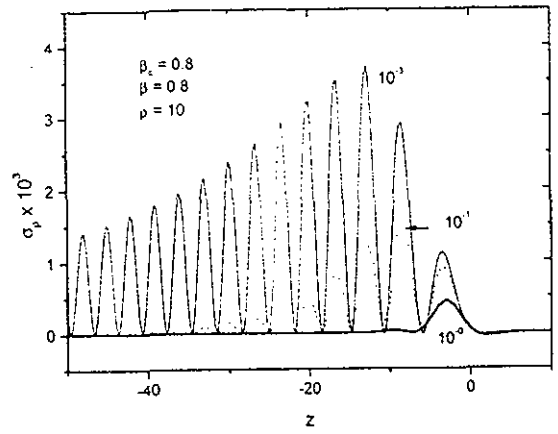

Figure 21: Shows how the inclusion of the imaginary part of ϵ affects the energy flux distribution. The number of a particular curve means the parameter p. The charge velocity is $\beta = 0.8$.

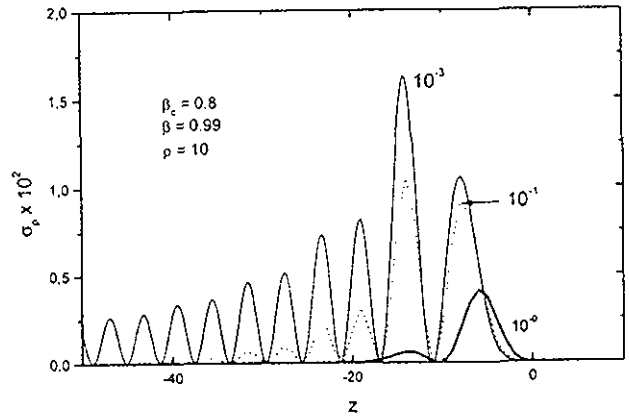

Figure 22: The same as in Fig. 21 but for the charge velocity $\beta = 0.99$. Comparing this figure with Figs. 18-21 we observe that the switching on the imaginary part of ϵ affects lesser for larger β.

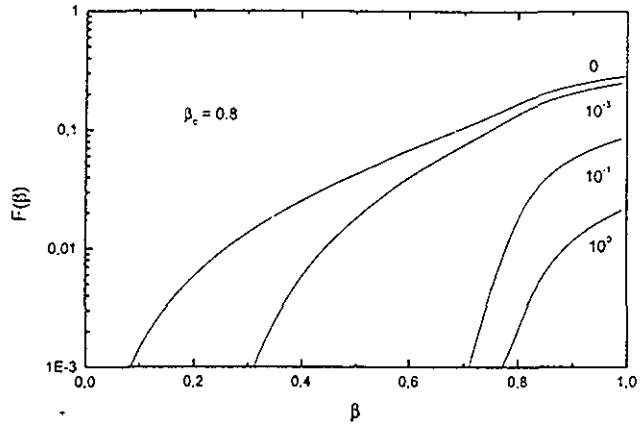

Figure 23: Shows how the inclusion of the imaginary part of ϵ affects the total energy losses W per unit length. The number of a particular curve means the parameter p; W and p are in units $e^2\omega_0^2/c^2$ and ω_0, resp.

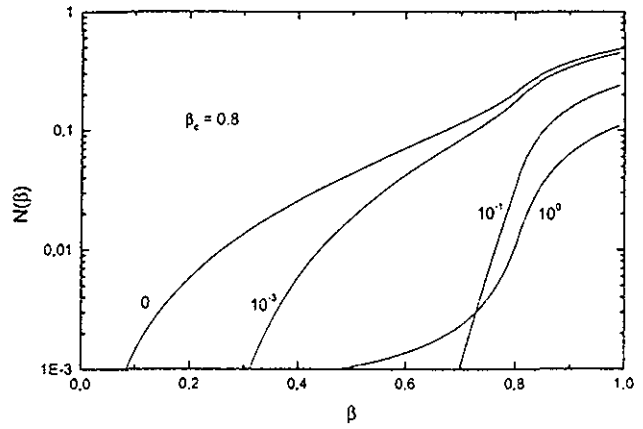

Figure 24: The number of quanta emitted in the radial direction per unit length (in units $e^2\omega_0/\hbar c^2$) as a function of the charge velocity β for different values of the parameter p.

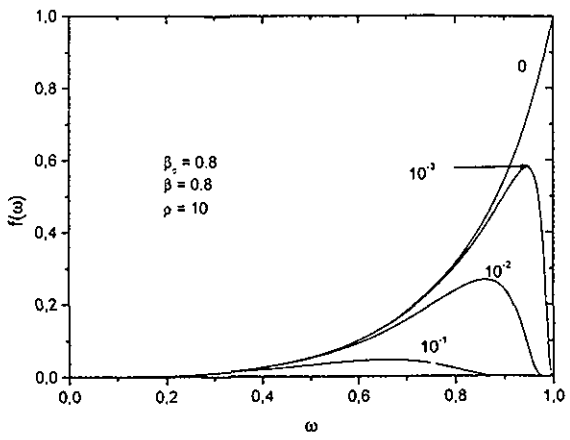

Figure 25: Spectral distribution of the energy losses (in units $e^2\omega_0/c^2$); ω is in units ω_0. The number of a particular curve means the parameter p.

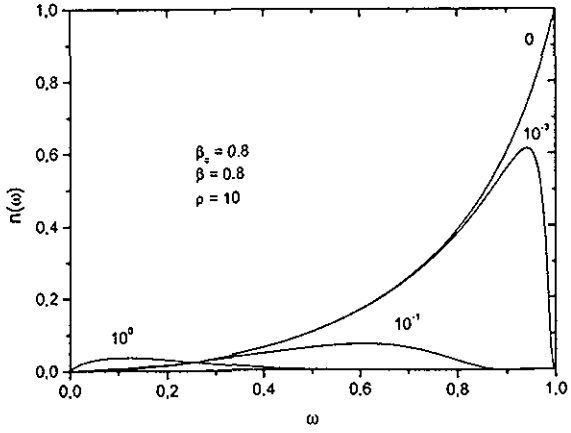

Figure 26: Spectral distribution of the emitted quanta (in units $e^2/\hbar c^2$); ω is in units ω_0. The number of a particular curve means the parameter p.

References

[1] Cherenkov P.A., 1934, *Dokl. Acad. Nauk SSSR*, **2**, 457.

[2] Frank I. and Tamm I., 1937, *Dokl. Acad. Nauk SSSR*, **14**, 107.

[3] Heaviside D., 1912, *Electromagnetic Theory*, vol. 3, (London, The Electrician).

[4] Volkoff G.M., 1963, *Amer. J. Phys.*, **31**, 601.

[5] Zin G.N., 1961, *Nuovo Cimento*, **22**, 706.

[6] Afanasiev G.N., Beshtoev Kh.M. and Stepanovsky Yu.P., 1996, *Helv. Phys. Acta*, **62**, 11.

[7] Frank I.M. 1988, *Vavilov-Cherenkov Radiation*, Moscow, Nauka.

[8] Born M. and Wolf E., 1975, *Principles of Optics*, (Oxford, Pergamon).

[9] Brillouin L., 1960, *Wave Propagation and Group Velocity*, (New York and London, Academic Press).

[10] Lagendijk A. and Van Tiggelen B.A., 1996, *Physics Reports*, **270**, 143.

[11] Fermi E., 1940, *Phys. Rev.*, **57**, 485.

[12] Bohr N., 1913, *Phil. Mag.*, **25**, 10; 1915, *Phil. Mag.*, **30**, 581.

[13] Ryazanov M.I., 1984, *Electrodynamics of Condensed Matter*, (Moscow, Nauka), in Russian.

[14] Afanasiev G.N. and Kartavenko V.G., 1997, *JINR Preprint E4-97-393*,Dubna.

[15] Ruzicka Ya. and Zrelov V.P., 1992, *JINR Preprint P1-92-233* , Dubna.

[16] Ruzicka Ya., 1993, *Theoretical and Experimental Investigations of the Vavilov-Cherenkov Effect* , Doctor of Science Dissertation, Dubna.

[17] Zrelov V.P., Ruzicka J. and Tyapkin A.A., 1998, *Pre-Cerenkov Radiation as Manifestation of the "Light Barrier"* , *JINR Rapid Communications*, 1[87]-98,23.

[18] Akhiezer A.I. and Shulga N.F., 1993, *High Energy Electrodynamics in Medium*, (Moscow, Nauka), In Russian.

[19] James M.B. and Griffithhs D.J., 1992, *Amer. J. Phys.*, **60**, 309.

[20] Diamond J.D., 1995, *Amer. J. Phys.*, **63**, 179.

[21] Bart G. de Grooth, 1997, *Amer. J. Phys.*, **65**, 1156.

[22] Gradshteyn I.S. and Ryzik I.M., 1965, *Tables of Integrals, Series and Products*, (New York, Academic Press).

[23] Sternheimer R.M., 1953, *Phys. Rev.*, **91**, 256.

[24] Gingburg V.L., 1996, *Usp. Fiz. Nauk*, **No 10**, 1033.

[25] Tamm I.E., 1939, *J. Phys. USSR*, **1**, No 5-6, 439.

[26] Bolotovsky B.M., 1957, *Usp. Fiz. Nauk*, **42**, 201.

[27] Zrelov V.P., 1970, *Vavilov-Cherenkov Radiation in High-Energy Physics*, (Jerusalem, Israel Program for Scientific Translations).

[28] Afanasiev G.N. and Eliseev S.M., 1997, *JINR Preprint E4-98-34* , Dubna.

[29] Migdal A.B., 1975, *Qualitative Methods in Quantum Theory*, (Moscow, Nauka), in Russian.

[30] Landau L.D. and Lifshitz E.M, 1992, *Electrodynamics of Continuous Media*, (Moscow, Nauka), in Russian.

Received by Publishing Department
on April 20, 1998.